Hindawi
Journal of Sensors
Volume 2019, Article ID 6437431, 7 pages
https://doi.org/10.1155/2019/6437431

Research Article

Hydrogen Sulfide Detection in the Midinfrared Using a 3D-Printed Resonant Gas Cell

Oscar E. Bonilla-Manrique,[1] **Harald Moser**,[2] **Pedro Martín-Mateos**,[1] **Bernhard Lendl**,[2] **and Marta Ruiz-Llata**[1]

[1]*Electronics Technology Department, Carlos III University of Madrid, Leganés 28911, Spain*
[2]*Institute of Chemical Technologies and Analytics, Vienna University of Technology, Vienna 1060, Austria*

Correspondence should be addressed to Oscar E. Bonilla-Manrique; obonilla@ing.uc3m.es

Received 7 December 2018; Revised 27 January 2019; Accepted 5 February 2019; Published 14 March 2019

Academic Editor: Vincenzo Spagnolo

A fast and reliable photoacoustic (PA) sensor for trace gas detection is reported. The sensor is based on a 3D-printed resonant cell in combination with a continuous wave mode-hop-free external cavity quantum cascade laser to rapidly acquire gas absorption data in the midinfrared range. The cell is designed so as to minimize the window PA background at a selected acoustic resonance. The goal is a resonant PA cell capable of detecting the traces of gases using wavelength modulation of the laser source and second harmonic detection. The versatility and enhancement of the limit of detection at sub-ppm levels are investigated by monitoring specific lines of hydrogen sulfide (H_2S). The noise-equivalent absorption normalized to laser-beam power and detection bandwidth is 1.07×10^{-8} W cm^{-1} Hz$^{-1/2}$ for H_2S targeting the absorption line at 1247.2 cm^{-1}. These properties make the sensor suitable for various practical sensors for water quality applications.

1. Introduction

Hydrogen sulfide (H_2S) is a very flammable, toxic, and corrosive gas. It is commonly found in the oil and gas industries, volcanic gases, thermal waters, and as a result of the microbial breakdown of organic matter. It is a water pollutant in groundwater supplies [1], wastewater, and sewer systems [2] relevant to prevent due to health and corrosion problems. Also, the presence of H_2S is a cost-effective option for assessing the vulnerability of water supplies to microbial contamination in developing settings [3].

Therefore, the implementation of sensitive and selective sensors and on-line monitoring systems is very important for water quality assessment as an alternative option to sparse water sample collection and laboratory analysis using conventional analysis techniques, such as gas chromatography. H_2S is a very volatile water soluble gas, so the detection is typically done in the gas phase. A number of different methods for H_2S detection have been developed and validated [4], including photoacoustic spectroscopy (PAS) [5]. This method provides a direct measurement of the optical absorption of the gas sample which depends on the concentration of H_2S. PAS techniques present the advantages of spectroscopic methods, such as a high sensitivity, a low limit of detection, and a very high selectivity to the specific target gas compared to other detection method, such as metal-oxide semiconductor, polymer conductive, and electrochemical sensors [4] with the additional advantages of low-sampling volumes [6] and robustness against environmental condition if all optical detection is used [7], compared with other spectroscopic techniques.

The PAS technique is based on measuring the acoustic pressure oscillation (photoacoustic response) that is originated due to the absorption of gas molecules inside a gas cell that is illuminated with a modulated laser beam either amplitude or wavelength. Better sensitivities and limits of detection can be achieved using resonant photoacoustic cells with laser modulation frequencies tuned to a specific mode of the resonant cell [5]. Typically, the resonant component of the gas cell is metallic [5, 8]. In this work, we evaluate the

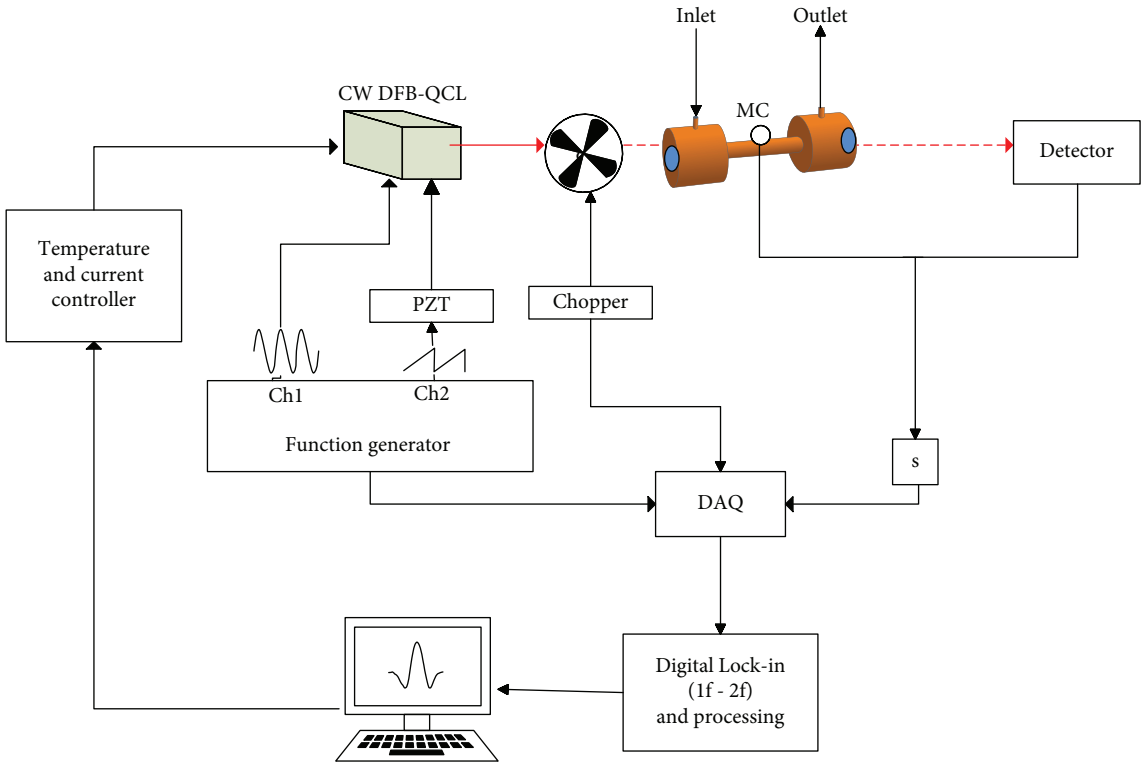

Figure 1: Experimental measurement setup: CW DFB-QCL, quantum cascade laser; PZT, piezoelectric controller; MC, microphone; DAQ, data acquisition; and s, selector.

performance of a PAS sensor using 3D printing to fabricate photoacoustic cells using materials resistant to H_2S corrosion. The sensor is evaluated with a light source in the midinfrared (MIR) due to the advantages of higher absorption peaks in this region of the spectrum and the increasing availability and functionality of MIR lasers, such as quantum cascade lasers (QCLs) and interband cascade lasers (ICLs) [9].

2. Materials and Methods

The system used in this study is based on a classic photoacoustic spectroscopy experiment, where an amplitude or wavelength modulated optical signal illuminates the gas sample inside of a cell and the generated acoustic wave is detected by a microphone installed in the cell. The experimental set-up is represented in Figure 1. In this set-up, amplitude modulation of the optical beam using an external chopper is used for gas cell characterization while wavelength modulation of the emitter is used for H_2S measurements as described below.

For trace gas detection, the photoacoustic signal, $S_{PA}(f)$, measured by the microphone depends linearly on several parameters, as described by:

$$S_{PA}(f) = S_m * P * \alpha(\lambda) * C, \quad (1)$$

where S_m is the sensitivity of the microphone, P is the optical power of the incident radiation, $\alpha(\lambda)$ is the absorption coefficient that is proportional to the gas concentration and depends on the wavelength, and C is the cell constant that depends on the geometry of the acoustic cell and the modulation frequency f [10]. In the following sections, the elements of the set-up that define the relevant parameters in equation (1) are described in detail.

2.1. Laser Source. A continuous wave mode-hop-free external cavity quantum cascade laser (CW MHF EC-QCL) model MHF-41078 from Daylight Solutions was used as the emitter. This laser has a center wavelength of 7.93 μm (1268 cm^{-1}), tuning range from 7.64 μm to 8.22 μm (1319 cm^{-1} to 1217 cm^{-1}), line width of 3×10^{-3} cm^{-1} (two orders of magnitude narrower than the spectral lines targeted in our experiments), and maximum output power of 180 mW and requires external water cooling. In the CW MHF EC-QCL model, the angular position of the internal grating is controlled via the built-in stepping motor that allows to set the emission wavelength near a specific absorption line of the target gas with a minimum step of 0.01 cm^{-1} (1001-TLC, tunable QCL controller, Daylight Solutions). A fine wavelength tuning within a range of up to 1.0 cm^{-1} can be achieved through an externally driven piezoelectric (PZT) controller (MDT6894A, Thorlabs) that is installed in the drive train to mechanically modulate the grating. This PZT allows emission wavelength modulation at maximum frequencies of tens of hertz. Higher modulation frequencies, up to 2 MHz, are possible via direct modulation of the CW MHF EC-QCL bias current. The maximum wavelength modulation depth is obtained via sinusoidal current modulation using an external input with an amplitude of 5 V; however, as precaution, the amplitude of this input was set to 4.5 V, which

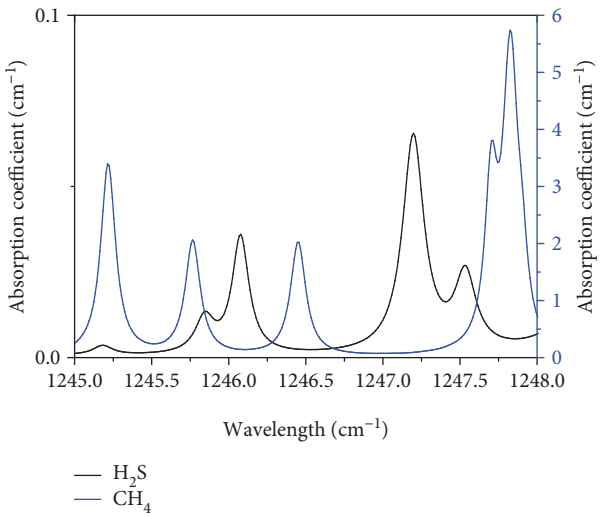

FIGURE 2: Simulation of the absorption spectra of pure CH_4 and H_2S using the HITRAN database. The pressure is set to 1 atm and the temperature to 296 K.

corresponds to a wavelength modulation depth of 0.065 cm^{-1} as previously characterized [11].

Figure 2 shows the absorption spectra of the gases used for the experiments: the target gas hydrogen sulfide (H_2S) and, a less toxic gas, methane (CH_4) for cell characterization. These reference spectra were calculated at atmospheric pressure based on the HITRAN2012 database [12]. The absorption peak at 1247.2 cm^{-1} was selected for H_2S detection, which corresponds to its rovibrational transitions of the $\nu 2$(A1) bending mode and is within the tuning range of the emitter. There is a close absorption peak for CH_4 at 1247.7 cm^{-1} which corresponds to the $\nu 4$(F2) bending mode of this molecule. Note that the peak absorption coefficient of CH_4 is two orders of magnitude higher than the peak for H_2S which is an advantage for cell calibration purposes.

According to equation (1), there are two methods to generate the photoacoustic signals. The first method consists of the amplitude modulation of the incident optical power from the CW MHF EC-QCL by an external chopper. The second method consists of the wavelength modulation of the laser via injection current modulation. As the emission wavelength varies around the absorption peak, a maximum acoustic signal can be detected at twice the modulation frequency (2-f WMS). It has been shown that the optimum wavelength modulation depth is 2.2 [13]. As shown in Figure 2, selected H_2S absorption line presents a full width at half maximum (FWHM) of about 0.14 cm^{-1} at normal temperature and pressure, which means that the optimum wavelength modulation depth to optimize PAS signal is 0.3 cm^{-1}. This number is ~4.7 times higher than the modulation depth allowed by the emitter used in the experiment as described above.

2.2. Sensor Instrumentation. Figure 1 represents the apparatus for laser configuration (temperature and current controller, function generator, and PZT drivers) and for the detection, signal acquisition, and processing (photodetector, DAQ, and digital lock-in). The temperature and current controller set the coarse operating point of the EC QCL in the vicinity of the selected absorption line. To fine tune the emission wavelength and to sweep around the absorption line, the laser PZT controller was driven using a function generator (Ch2). To generate the photoacoustic signal in the gas sample, two modulation methods were implemented: amplitude modulation by means of a chopper (MC2000B with MC1F10HP chopper blade, Thorlabs) and wavelength modulation via laser current modulation from a function generator (Ch1). However, these two modulation methods were not used at the same time; amplitude modulation was used to calibrate the gas cell resonance, and wavelength modulation was used in the proposed system for H_2S detection. This system provided two output signals: the signal from a photodetector (PIP-DC-200M-F-M4, Vigo System) placed at the output of the gas cell for a direct measurement of the transmitted light through the gas sample and the signal from the microphone (FG-23329-P18, Knowles Electronics) placed at the center of the gas cell. The signals (acoustic, photodetector, and reference) were digitized with a DAQ (USB-1602HS, MC-Measurement Computing) with a 16-bit AD converter, 2MS/s sampling frequency, and external trigger. The data was processed with a LabVIEW program that implemented a digital lock-in amplifier of the two channels in real time.

The work point of the QCL was set at a laser temperature of 18°C, injection current of 400 mA, and emission wavelength around 1247 cm^{-1}. The optical signal illuminated the gas sample inside of the resonant cell installed at a distance of 200 mm, which maintained a constant spot size (2.5 mm) centered through the resonant gas cell.

Different target gases were used. The CH_4 was used for the characterization of the resonant cell due to its lower level of toxicity, ease of installation, and greater absorption at the selected wavelengths. The gas was directly supplied by a bottle at a concentration of 5% in volume. For the characterization of the system, the H_2S was used and the mixtures were established by a gas control system that met the on-site safety regulations. The different concentration levels, that ranged from 0 to 500 parts per million volume (ppmv), were prepared by N_2 (high purity) dilution from a 500 ppmv H_2S standardized gas bottle (matrix N_2) with a custom-made gas mixer, as shown in Figure 3. It was comprised of mass flow controllers, a pressure controller, and valves at a constant rate flow of 0.2 l/min.

2.3. Gas Cell Design. As shown in equation (1), the cell constant parameter, C, must be improved to obtain a greater photoacoustic signal. Therefore, a resonant gas cell (RGC) was designed and used in this system. The cell constant, C, is given by:

$$C = \frac{G * (\gamma - 1) * l * Q}{f * V}, \tag{2}$$

where f is the frequency of the acoustic signal, G is a geometrical correction factor, γ is the specific heat, Q is the quality factor of the acoustic resonance selected to perform the

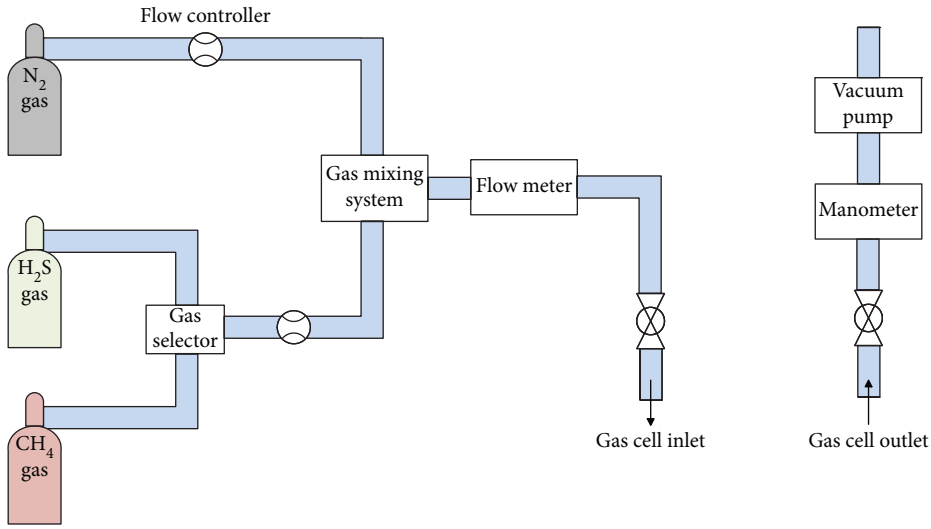

Figure 3: Block diagram of the gas mixing.

measurements, V is its volume, and l is the length. This equation shows that one of the relevant parameters is the gas cell cavity section (V/l). The quality factor, Q, is defined by:

$$Q = \frac{f}{\Delta f}, \tag{3}$$

where f is a resonance frequency and Δf is the FWHM of the acoustic resonance.

Different designs of resonant photoacoustic cells have been proposed [14–18]. The reference cell design that was used in this study is represented in Figure 5. It consists of a cylinder resonator (a pipe) terminated at both ends with two-cylinder buffer volumes, where the gas inlet/outlet connectors and the optical windows were installed. A resonant gas cell with buffer was chosen due to the reduction of the flow and acoustic noise. The acoustic detector was a microphone that was installed in the middle of the cylinder resonator.

The first design parameter was the geometrical dimensions of the pipe (radius, r, and length, l). The objective was to achieve a resonance of about 2 kHz, which is within the bandwidth of the microphone and large enough to reduce the 1/f electronic and ambient acoustic noise. Equation (4) shows the frequency of resonance in a cell open on both sides [17]:

$$f_r = \frac{n * c}{2 * (l + \Delta l)}, \tag{4}$$

where c is the sound velocity, n the mode number, and l is the length of the cell. A correction has to be included for the open-end resonator and can be approximated as an elongation of the resonator by $\Delta l \approx 0.6r$ [17].

As shown by equation (2), the best C is achieved for a long cell with a small radius ($l >> r$). Thus, the diameter of the cell was decided to be 5 mm ($r = 2.5$ mm), since this size is slightly larger than the laser spot (2.5 mm), and it is sufficient to obtain smooth surface. Therefore, from equation (4) and assuming sound velocity (c) at standard conditions for air, the resulting resonator length was 88 mm.

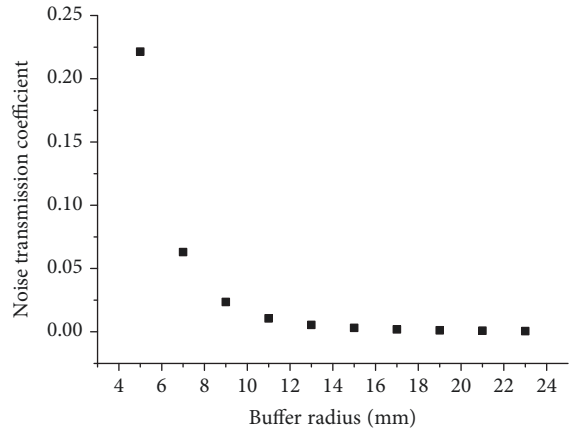

Figure 4: Noise transmission coefficient at different buffer radiuses ($l_b = 44$ mm).

To attenuate the noise due to cell optical windows absorption and turbulence noise in the gas inlet and outlet, two buffer volumes are considered as acoustic filters at both ends of resonator. The optimal dimensions of the buffer were calculated using the noise transmission coefficient (NTC), as described by equation (5) [18]:

$$\mathrm{NTC} = \frac{4}{4\ \cos^2 Kl_b + \left(\left(S_b/S_r\right) + \left(S_r/S_b\right)\right)^2 \sin^2 Kl_b}, \tag{5}$$

where S_r is resonator cross section, l_b and S_b are the length and cross section of the buffer, respectively, and K is the acoustic wave number. The minimum and maximum values of the NTC can be calculated by assigning $(2n + 1)\pi/2$ and $n\pi$ to Kl_b in equation (5), respectively. Thereby, the minimum noise transmission is obtained for a buffer volume with a length of a quarter of the acoustic wavelength ($\lambda/4$). Figure 4 illustrates the NTC as a function of the buffer radius

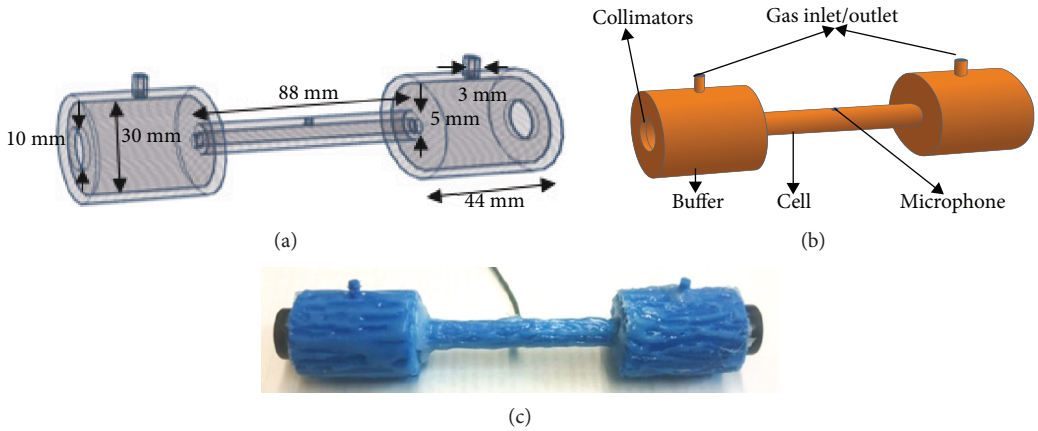

Figure 5: Resonant gas cell: (a) structure and dimensions of the resonant gas cell (in mm), (b) 3D design including all additional cell part, and (c) 3D-printed resonant gas cell.

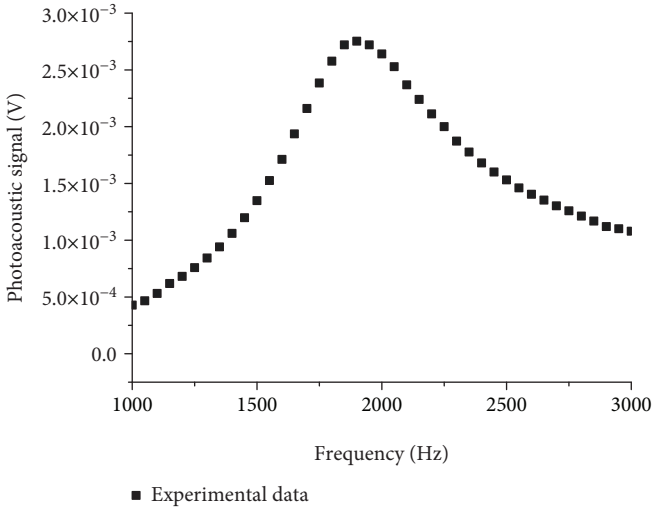

Figure 6: Photoacoustic signal under different modulation frequencies, from 1 to 3 kHz, when the laser wavelength was set at 1247.7 cm^{-1} in the absorption line of CH_4.

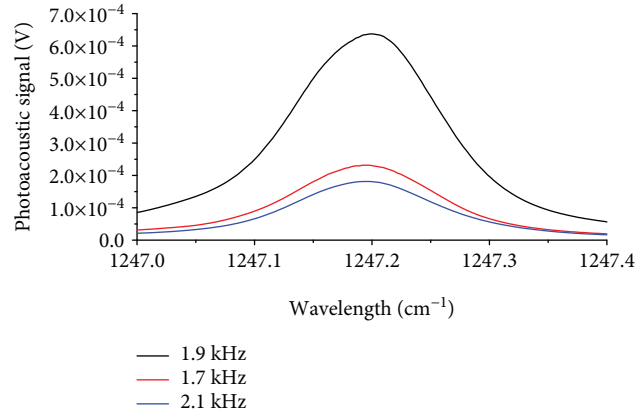

Figure 7: Photoacoustic signal when pump laser is tuned across the absorption line of H_2S at 1247.2 cm^{-1} with different amplitude modulation frequencies. Black line: modulation frequency is 1.9 kHz. Red line: modulation frequency is 1.7 kHz. Blue line: modulation frequency is 2.1 kHz.

given a $\lambda/4$ buffer length (44 mm). It can be seen that increasing the radius above 15 mm does not improve the NTC. Thereby, the $\lambda/4$ buffer volumes had a length of 44 mm, and diameter of 30 mm (r_b = 15 mm).

Figure 5(a) shows the resulting cell dimensions; further, the cell design includes two optical windows, the placement of the microphone and the gas inlet and outlet (Figure 5(b)). The 3D-printed version (Figure 5(c)) was built as a high-quality monolithic piece (layer height of 0.05 mm to obtain a surface as smooth as possible) in a common thermoplastic polymer as acrylonitrile butadiene styrene (ABS). This has a greater thermal, chemical, and mechanical resistance than other plastics such as polylactide (PLA) [19]. It was covered with a waterproofing coating of ~3 mm to prevent leakage in the joints with the windows and the sensor by means of an adhesive composed of ethylene vinyl acetate. Two calcium fluoride-wedged windows were installed (CaF2) (Ø1/2" wedged CaF2 window, uncoated, Thorlabs) for optical input and output. The advantage of having the output window is that it allowed direct absorption detection at the same time as the acoustic detection. The microphone (FG-23329-P18, Knowles Electronics) was used as an acoustic detector and had a 3 mm diameter and sensitivity of -53 db at cell resonant frequency. It was drilled through the resonator, and the surface of the microphone was installed flush with the resonator wall to efficiently detect the acoustic wave.

3. Results and Discussion

3.1. Resonant Gas Cell Characterization. Methane was used to verify the resonant frequency of the gas cell. First, the absorption spectrum of the CH_4 was verified by a direct absorption measurement using the photodetector and a high concentration of the target gas (the gas cell was filled with 5% CH_4 at 24°C and atmospheric pressure). The laser was tuned from 1247 cm^{-1} to 1249 cm^{-1} by controlling the angular position of the internal EC grating using the QCL controller. The obtained absorption trace was compared to the reference absorption profile obtained from the HITRAN database (Figure 2) in order to calibrate the QCL controller. Once

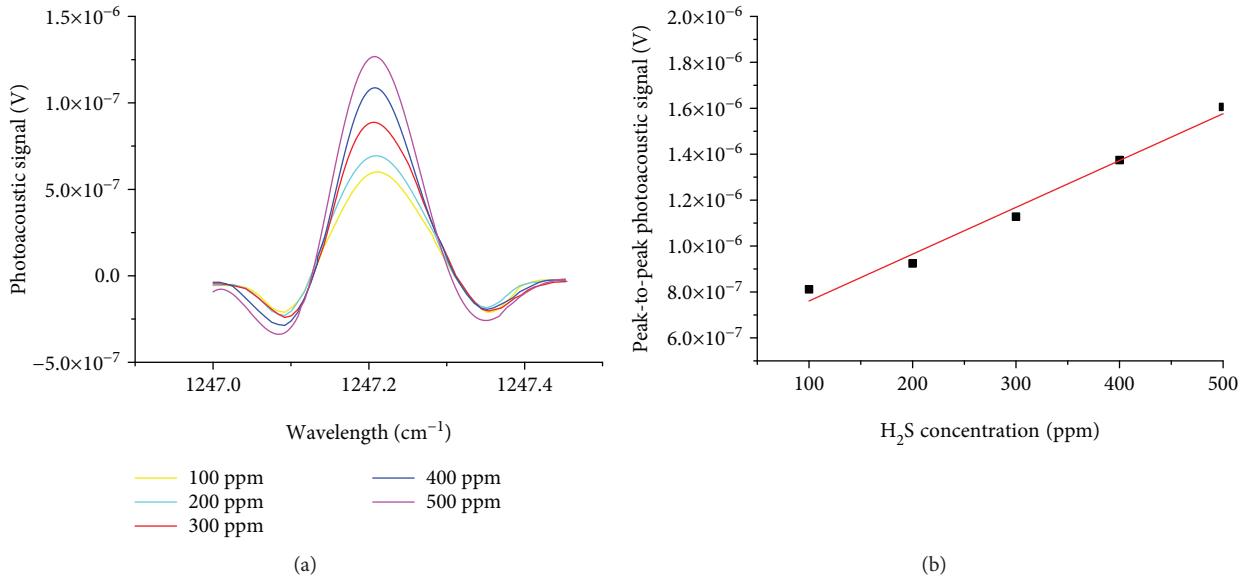

FIGURE 8: Second harmonic signal: (a) when the pump laser was tuned across the absorption line of H_2S at 1247.2 cm^{-1} and (b) for the peak-to-peak amplitude of the second harmonic for a sample gas mixture from 100 ppm to 500 ppm at 1 bar of pressure and room temperature.

the laser control parameters were obtained, the laser wavelength was set at 1247.7 cm^{-1} and the intensity modulation was generated by the mechanical chopper. The frequency modulation was changed in the range of 1 to 3 kHz to characterize the resonant gas cell (Figure 6). The maximum peak for the photoacoustic signal was identified at a frequency of 1.9 kHz, and a quality factor of 2.5 was obtained for the 3D-printed cell.

3.2. Low Concentration Detection of H_2S. The H_2S was used to validate the performance of the PAS system. Hence, the CW MHF EC-QCL was tuned to the selected absorption line of H_2S at 1247.2 cm^{-1}. The effective optical power emitted was 50 mW, taking into account the 90% transmission efficiency of the windows. The metal gas cell was filled with 500 ppm H_2S balanced by nitrogen at atmospheric pressure and room temperature (24°C). The external cavity grating was modulated with a saw tooth waveform at 10 mHz in a range to cover the H_2S absorption line. The photoacoustic signal generated via intensity modulation of the laser by means of the chopper was measured for three different frequencies (1.7, 1.9, and 2.1 kHz), and the responses are shown in Figure 7. This test allowed us to confirm the resonant frequency of the 3D-printed resonant cell and also to identify the absorption peak at 1247.2 cm^{-1} and a FWHM of 0.15 cm^{-1} at atmospheric pressure.

The sensor sensitivity was investigated for mixtures of H_2S from 100 ppm to 500 ppm. In order to avoid the external chopper, the photoacoustic signal was generated via direct sinusoidal current modulation of the laser at 1.9 kHz. As the system operated at atmospheric pressure, it worked below the optimal modulation index (the optimum modulation depth was shown to be 2.2 times the width of the absorption line [13]). The output from the microphone was digitized with a DAQ and processed by a digital lock-in amplifier at its second harmonic frequency. The lock-in integration time was set to 0.3 s. The second harmonic lock-in outputs (2f signal) for different concentrations is shown in Figure 8, where a linear fit of the data demonstrates good linearity for the sensor.

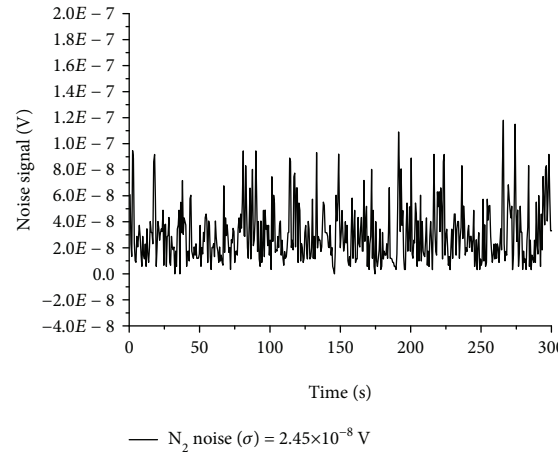

FIGURE 9: Noise signal for the acquired 2f-WMS signal for pure N_2.

The noise of the acquired 2f-WMS signal for pure N_2 was measured during 5 minutes as is plotted in Figure 9. The standard deviation (σ) of the noise was 2.45×10^{-8} V. The determined signal-to-noise ratio (SNR) for 100 ppm was ~33. Hence, the corresponding normalized noise equivalent absorption (NNEA) coefficient for H_2S was 1.07×10^{-8} W cm^{-1} $Hz^{-1/2}$ with a filter slope of 18 dB/oct, this gives a lower detection limit for a signal to noise ratio of unity (SNR = 1) of 0.3 ppm for a typical time constant of 30 s.

4. Conclusions

In this paper, a photoacoustic sensor was presented that was based on the fast, low cost, compact, and reliable

design of a resonant gas cell that can be fabricated using 3D-printing techniques. The use of plastic gas cells manufactured in materials such as high-impact polystyrene (HIPS) would allow the work in corrosive environments, such as in the presence of H_2S, due to its chemical resistance, machinability, and low cost. The potential was demonstrated in the low-level detection of H_2S at standard conditions of temperature and pressure, which may be relevant in the development of a practical monitoring device for the wastewater or leachate treatment industry, as well as for the environmental monitoring of hazardous gases.

A normalized noise equivalent absorption (NNEA) of 1.07×10^{-8} W cm^{-1} Hz$^{-1/2}$ and detection limit of 0.3 ppm (30 s sampling time) for H_2S were achieved. The sensor demonstrator used a continuous wave mode-hop-free external cavity quantum cascade laser (CW MHF EC-QCL) tuned at a specific absorption peak of H_2S whose wavelength was modulated via modulation of its injection current. The amplitude of this modulation was limited by the laser and its instrumentation to a modulation index of ~0.5 of the FWHM of the abortion line at standard conditions. A more compact version of the H_2S PA sensor would be implemented using a single wavelength QCL whose typical tuning range via injection current is above 2 cm^{-1}. Such kind of laser would allow an optimal modulation index of 2.2 and thus the PA signal improvement by a factor of 3 [13].

Data Availability

The data used to support the findings of this study are included within the article.

Conflicts of Interest

The authors declare that there is no conflict of interest regarding the publication of this paper.

Acknowledgments

This work was supported by the Spanish Ministry of Economy and Competitiveness (grant TEC-2014-52147-R (MOSSI) and grant TEC2017-86271-R (PARAQUA)) and by the Carlos III University of Madrid (grant for the mobility of researchers).

References

[1] S. H. C. Onsumption, T. Rade, and F. I. I. N. I. Taly, "Elevated hydrogen sulfide concentrations in groundwater," *Occupational Health & Safety*, pp. 2004-2005, 2008.

[2] J. H. Ko, Q. Xu, and Y.-C. Jang, "Emissions and control of hydrogen sulfide at landfills: a review," *Critical Reviews in Environmental Science and Technology*, vol. 45, no. 19, pp. 2043–2083, 2015.

[3] R. S. Khush, B. F. Arnold, P. Srikanth et al., "H_2S as an indicator of water supply vulnerability and health risk in low-resource settings: a prospective cohort study," *The American Journal of Tropical Medicine and Hygiene*, vol. 89, no. 2, pp. 251–259, 2013.

[4] S. K. Pandey, K. H. Kim, and K. T. Tang, "A review of sensor-based methods for monitoring hydrogen sulfide," *TrAC Trends in Analytical Chemistry*, vol. 32, pp. 87–99, 2012.

[5] S. Manohar and D. Razansky, "Photoacoustics: a historical review," *Advances in Optics and Photonics*, vol. 8, no. 4, pp. 586–617, 2016.

[6] S. Zhou, M. Slaman, and D. Iannuzzi, "Demonstration of a highly sensitive photoacoustic spectrometer based on a miniaturized all-optical detecting sensor," *Optics Express*, vol. 25, no. 15, pp. 17541–17548, 2017.

[7] Q. Wang and Q. Yu, "Polymer diaphragm based sensitive fiber optic Fabry-Perot acoustic sensor," *Chinese Optics Letters*, vol. 8, no. 3, pp. 266–269, 2010.

[8] T. Rück, R. Bierl, and F.-M. Matysik, "Low-cost photoacoustic NO_2 trace gas monitoring at the pptV-level," *Sensors and Actuators A: Physical*, vol. 263, no. 2, pp. 501–509, 2017.

[9] T. K. Subramaniam, "Quantum cascade laser in atmospheric trace gas analysis," *Journal of Environment*, vol. 1, no. 1, pp. 1–4, 2015.

[10] C. Haisch, "Photoacoustic spectroscopy for analytical measurements," *Measurement Science and Technology*, vol. 23, no. 1, article 012001, 2012.

[11] M. Helman, H. Moser, A. Dudkowiak, and B. Lendl, "Off-beam quartz-enhanced photoacoustic spectroscopy-basedsensor for hydrogen sulfide trace gas detection using a mode-hop-free external cavity quantum cascade laser," *Applied Physics B: Lasers and Optics*, vol. 123, no. 5, pp. 1–8, 2017.

[12] L. S. Rothman, I. E. Gordon, Y. Babikov et al., "The HITRAN2012 molecular spectroscopic database," *Journal of Quantitative Spectroscopy and Radiative Transfer*, vol. 130, pp. 4–50, 2013.

[13] S. Schilt and L. Thévenaz, "Wavelength modulation photoacoustic spectroscopy: theoretical description and experimental results," *Infrared Physics & Technology*, vol. 48, no. 2, pp. 154–162, 2006.

[14] A. Elia, P. M. Lugarà, C. di Franco, and V. Spagnolo, "Photoacoustic techniques for trace gas sensing based on semiconductor laser sources," *Sensors*, vol. 9, no. 12, pp. 9616–9628, 2009.

[15] J. Zhao, Z. Zhao, L. Du, and S. Wu, "Performance of the photoacoustic resonant cell remodified from Helmholtz cavity," *Applied Optics*, vol. 50, no. 25, p. 4936, 2011.

[16] Y. He, Y. Ma, Y. Tong, X. Yu, and F. K. Tittel, "HCN ppt-level detection based on a QEPAS sensor with amplified laser and a miniaturized 3D-printed photoacoustic detection channel," *Optics Express*, vol. 26, no. 8, pp. 9666–9675, 2018.

[17] A. Miklós, P. Hess, and Z. Bozóki, "Application of acoustic resonators in photoacoustic trace gas analysis and metrology," *The Review of Scientific Instruments*, vol. 72, no. 4, pp. 1937–1955, 2001.

[18] M. Tavakoli, A. Tavakoli, M. Taheri, and H. Saghafifar, "Design, simulation and structural optimization of a longitudinal acoustic resonator for trace gas detection using laser photoacoustic spectroscopy (LPAS)," *Optics and Laser Technology*, vol. 42, no. 5, pp. 828–838, 2010.

[19] B. M. Tymrak, M. Kreiger, and J. M. Pearce, "Mechanical properties of components fabricated with open-source 3-D printers under realistic environmental conditions," *Materials and Design*, vol. 58, pp. 242–246, 2014.